

- ¹⁶R. Fuchs, Phys. Rev. **111**, 387 (1958).
¹⁷Z. Khas, Czech. J. Phys. **B8**, 568 (1965).
¹⁸M. Trlifaj, Czech. J. Phys. **9**, 446 (1959); **B14**, 227 (1964); **B15**, 780 (1965).
¹⁹M. Gershenson and R. M. Mikulyak, Appl. Phys. Letters **8**, 245 (1966).
²⁰F. A. Trumbore, M. Gershenson, and D. G. Thomas, Appl. Phys. Letters **9**, 4 (1966).
²¹P. J. Dean, J. D. Cuthbert, D. G. Thomas, and R. T. Lynch, to be published.
²²D. F. Nelson, L. F. Johnson, and M. Gershenson, Phys. Rev. **135**, A1399 (1964).

MIXING OF VISIBLE AND NEAR-RESONANCE INFRARED LIGHT IN GaP

W. L. Faust and Charles H. Henry

Bell Telephone Laboratories, Murray Hill, New Jersey

(Received 3 November 1966)

Sum and difference frequency generation are observed when visible laser light is mixed in GaP with each of five infrared laser frequencies near the reststrahl. The measured infrared frequency dependence of the nonlinear susceptibility, which varies by a factor of 60, is accounted for by theory.

We have observed radiation at sum and difference frequencies upon mixing infrared and visible laser light in a GaP crystal. The mixing was observed for five different infrared (IR) laser frequencies (211.6, 303.7, 353.7, 357.5, and 428.0 cm^{-1}) lying near the lattice resonance (reststrahl) at 365 cm^{-1} . This enabled us to measure for the first time the variation of the nonlinear susceptibility as the infrared frequency passed through the reststrahl region. By making use of the relationship between spontaneous Raman scattering and frequency mixing, we have been able to account theoretically for the IR frequency dependence of the nonlinear susceptibility.

A Cassegrainian optical arrangement was employed to bring a 6328-Å He-Ne laser beam and the IR beam to a common focus on the surface of a room-temperature GaP crystal. The visible laser produced 150 to 300 mW, and the time-averaged powers in the IR laser lines were approximately 0.17 mW at 211.6 cm^{-1} , 0.43 mW, at 303.7 cm^{-1} , 0.04 mW at 353.7 cm^{-1} , 5.7 mW at 357.5 cm^{-1} , and 1.1 mW at 428.0 cm^{-1} . Both laser beams were limited to narrow cones about the 110 axis. We observed the light scattered in the forward 110 direction with a 2-meter Bausch and Lomb spectrograph, using both photography and gated photon counting (IR-synchronous) to record the intensities. The IR powers were measured with a Golay cell and a thermopile roughly calibrated for 30- μ radiation.

Figure 1(a) shows the dispersion curves for the IR-frequency waves which can propagate in a GaP crystal. Near the lattice resonance,

at $\omega_0 = 365 \text{ cm}^{-1}$, the transverse waves have both photon and phonon character. They are known as polaritons.¹ This experiment is an outgrowth of a previous one in which the polariton dispersion curve was plotted out experimentally from ω_0 to 307 cm^{-1} by the observation of spontaneous Raman scattering by polaritons.^{2,3} Frequency mixing can be viewed as spontaneous Raman scattering by polaritons, enhanced by increasing the population of some of the polariton modes at the IR frequency. Raman scattering and frequency mixing near the reststrahl involve the same nonlinearity parameters. We shall make use of this when we compute the frequency dependence of the nonlinear susceptibility.

Figure 1(b) is a densitometer trace of a plate showing the spectrum of the light forward scattered along the 110 direction. Peaks A, B, and C are due to spontaneous Raman scattering: A, forward scattering by the LO phonons; B, backward scattering by large wave-vector polaritons, accidentally observed because of crystal surface reflections; C, forward scattering by polaritons. Peak C occurs at the matching frequency where the wave-vector mismatch $\Delta k \equiv |\vec{k}_L - \vec{k}_S - \vec{q}| = 0$. Here \vec{k}_L , \vec{k}_S , and \vec{q} refer to the visible laser wave, the scattered wave, and the polariton, respectively. The peak is broad because the matching frequency changes with the scattering angle θ between \vec{k}_L and \vec{k}_S ; the collecting optics accepted a cone of scattered light with $0^\circ \leq \theta \leq 0.8^\circ$. The lines labeled by frequencies were present only when the IR laser was operating. The intensities of these lines $I(\omega_S)$ ranged over more

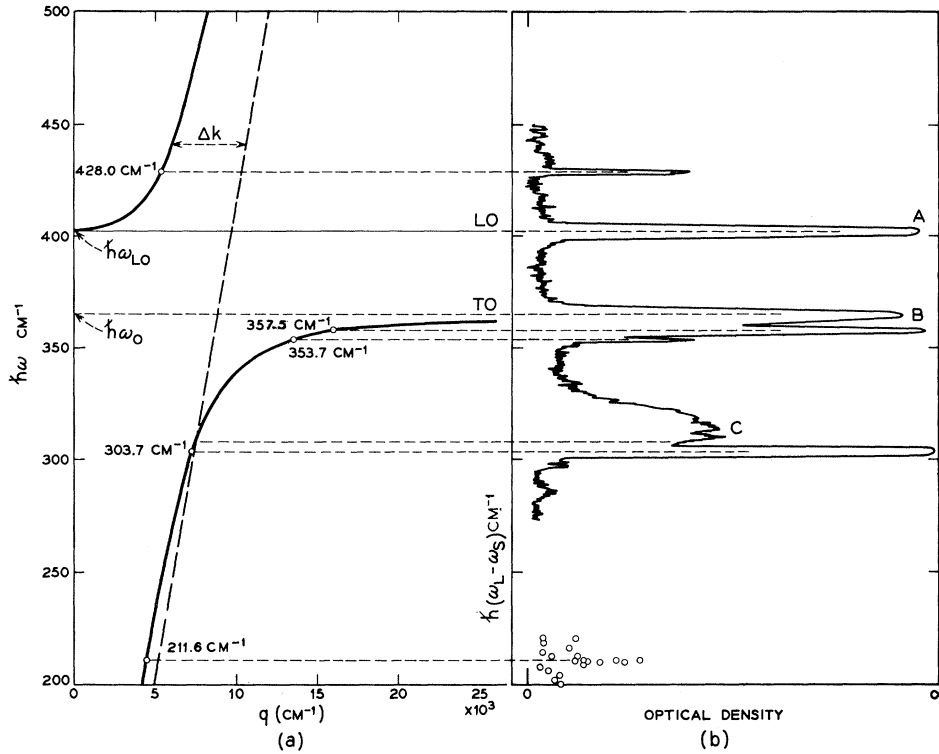


FIG. 1. (a) Solid curves, dispersion curves (ω vs q) of the polariton and the LO phonon. Dashed curve (line), plot of ω vs $|\vec{k}_L - \vec{k}_S|$ for forward ($\theta = 0^\circ$) scattering, $\vec{k}_L \parallel \vec{k}_S \parallel q$. The IR laser frequencies are indicated. (b) Densitometer trace of the spectrum of scattered light. A, B, and C are spontaneous Raman scattering. The lines at difference frequencies ($\omega_L - \omega$), which are instrumentally narrow, appear wide here because of the spectrograph slit width used (3 cm^{-1}). The line at 211.6 cm^{-1} is represented by photomultiplier data.

than three orders of magnitude. The line at $\omega_L - 303.7 \text{ cm}^{-1}$, which was nearly matched, was detectable in an exposure time of a few seconds. The line at $\omega_L - 211.6 \text{ cm}^{-1}$ could not be detected photographically in our longest exposure of two hours. In Fig. 1(b) this line is represented by photomultiplier data. The photographs of the difference frequencies reflected the spatial distribution of the focused IR laser beam. We saw evidence of TEM_{00q} and TEM_{01q} modes.

In frequency mixing experiments, the nonlinear polarization is conventionally written

$$P^{NL}(\omega_S) = d(\omega_S = \omega_L - \omega)E(\omega)E(\omega_L). \quad (1)$$

Here ω , ω_L , and ω_S are the IR laser, visible laser, and scattered mixing frequencies, respectively. We can study the IR frequency dependence of $|d|$ from the intensities at the several ω_S , since

$$I(\omega_S) \propto |d(\omega)|^2 [l_c(\omega)]^2 [n(\omega)]^{-1} I(\omega) I(\omega_L). \quad (2)$$

Here $I(\omega)$ is the IR power transmitted into the crystal, $n(\omega)$ is the real part of the refractive index, and $l_c(\omega)$ is the coherence length. In our cases, since the polariton field damps out before crossing the crystal,⁴

$$l_c(\omega) = \{[\Delta k(\omega)]^2 + [\frac{1}{2}\alpha(\omega)]^2\}^{-1/2}.$$

Here α^{-1} is the IR absorption length, and Δk has been defined earlier.⁵ An adequately accurate value for Δk for the nearly matched line at $\omega_L - 303.7 \text{ cm}^{-1}$ was found from a determination that $\Delta k = 0$ at $\omega = 307 \pm 1 \text{ cm}^{-1}$. This is the frequency at which the 0° Raman scattering was found to peak, under study with high angular resolution.

The measured values of $|d|$ are plotted in Fig. 2. No data were taken for the line at $\omega_L - 353.7 \text{ cm}^{-1}$. The solid curve is from a theoretical expression for $|d|$ which we shall proceed to develop. The experimental values were determined only within a constant factor, which

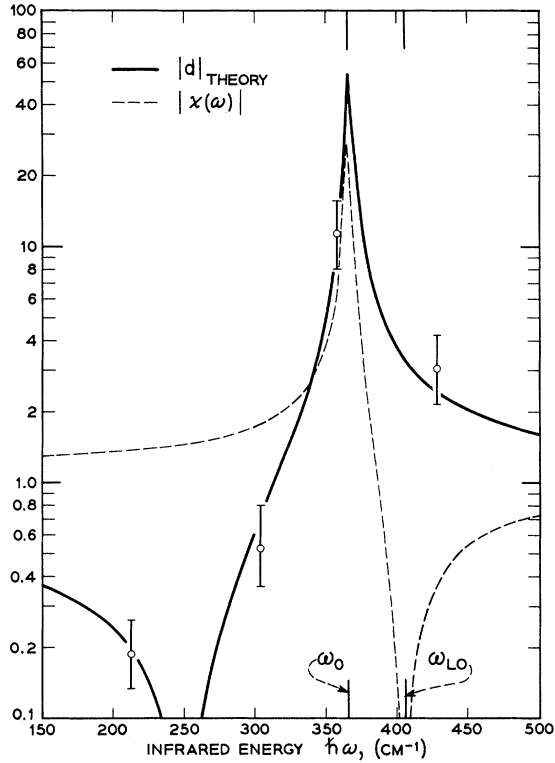


FIG. 2. The moduli of the nonlinear and the infrared linear susceptibilities, normalized to approach unity for large ω . The measured $|d|$ have been normalized for best fit to $|d|_{\text{theory}}$.

was adjusted for the best fit with theory. The agreement is excellent.

Associated with a polariton (also with an LO phonon) there are an electric field $\vec{E}(\omega)$ and an ionic displacement $\vec{Q}(\omega)$. It is useful to express the electric polarization (linear or nonlinear) as a function of these two variables. This approach has been used by Huang⁶ to discuss linear optical phenomena near the reststrahl, by Poulet⁷ to discuss Raman scattering in piezoelectric crystals, and by Kleinman⁸ to discuss nonlinear optics in general. First-order Raman scattering and frequency mixing arise because the electric susceptibility is a linear function of $\vec{E}(\omega)$ and $\vec{Q}(\omega)$. This gives rise to a nonlinear polarization at $\omega_S = \omega_L - \omega$:

$$P_z^{NL}(\omega_S) = [d_E E_y(\omega) + d_Q Q_y(\omega)] E_x(\omega_L). \quad (3)$$

Here x, y , and z are the 100 axes of the cubic crystal.⁹ We assume that d_E and d_Q are real and essentially constant over the IR frequen-

cy range of interest in this experiment. Our justification for this is that the derivation of Eq. (3) from a general classical model shows that d_E and d_Q may be so regarded provided that ω_L and ω_S are each well removed from resonant frequencies of the crystal, i.e., the lattice frequency and the band-gap frequencies.

$E_y(\omega)$ and $Q_y(\omega)$ are related by the lattice equation of motion

$$M(\omega_0^2 - \omega^2 - i\omega\Gamma)Q(\omega) = e_L E(\omega). \quad (4)$$

In GaP, $\Gamma \approx 0.01\omega_0$ at room temperature. Equation (4) shows that if $Q(\omega)$ and $E(\omega)$ are in phase for $\omega < \omega_0$, they are out of phase for $\omega > \omega_0$. There is constructive or destructive interference in the net radiation, which $\propto |d_Q Q(\omega) + d_E E(\omega)|^2$. Using Eqs. (1), (3), and (4), we can express the IR frequency dependence of the nonlinear susceptibility as

$$d(\omega_S = \omega_L - \omega) = d_E \left[1 + C \left(1 - \frac{\omega^2}{\omega_0^2} - \frac{i\omega\Gamma}{\omega_0^2} \right)^{-1} \right]. \quad (5)$$

We evaluate the constant $C = d_Q(d_E)^{-1}e_L M^{-1} \times (\omega_0)^{-2}$ from the ratio of the intensities of the LO and TO Raman scattering measured at $\theta = 90^\circ$. These intensities are $\propto |d_E E(\omega) + d_Q Q(\omega)|^2$ evaluated, respectively, at $\omega = \omega_{LO} = 403 \text{ cm}^{-1}$ and at $\omega = \omega_{TO} = \omega_0 = 365 \text{ cm}^{-1}$. In this expression we eliminate $E(\omega)$ using Eq. (4). For Stokes-Raman scattering the proper value of $Q^2(\omega)$ is $(\hbar/2M\omega)(n+1)$, where n is the Bose-Einstein occupation number at room temperature.¹⁰ The ratio $I(\omega_{LO})$ to $I(\omega_0)$ is 1.73 ± 0.05 . We find $C = -0.53 \pm 0.03$.¹¹ Using this value in Eq. (5), we have plotted $|d|$ vs ω in Fig. 2. Note that $|d|$ approaches zero near 250 cm^{-1} because of cancellation of the two contributions to $P^{NL}(\omega_S)$.

We have also tried to fit our data to an empirical rule found by Miller,¹² which accounts remarkably well for the large variations in $|d|$ measured in different materials. In our experiment, Miller's rule predicts that d will have the same infrared frequency dependence as the linear infrared electric susceptibility $\chi(\omega)$. Our measurements are in sharp disagreement with this prediction. $\chi(\omega)$ and $d(\omega_S = \omega_L - \omega)$ are each a sum of two terms, a nonresonant term and a resonant term $\propto Q(\omega)/E(\omega)$. For $\omega < \omega_0$ these two terms contribute constructively to $\chi(\omega)$, but destructively to $d(\omega_S = \omega_L - \omega)$.

We acknowledge helpful discussions with C. G. B. Garrett, J. J. Hopfield, D. A. Klein-

man, R. Loudon, R. C. Miller, and D. E. McCumber. We wish to thank A. S. Barker for infrared measurements and D. MacNair for overcoming cathode problems with the IR laser. We thank R. H. Eick and J. A. May for technical assistance.

¹J. J. Hopfield, Phys. Rev. **112**, 1555 (1958).

²C. H. Henry and J. J. Hopfield, Phys. Rev. Letters **15**, 964 (1965).

³S. P. S. Porto, B. Tell, and T. C. Damen, Phys. Rev. Letters **16**, 450 (1966), have made a similar measurement in ZnO.

⁴Our crystal was 3.9 absorption lengths thick at 211.6 cm^{-1} . The damping was greater at the other IR frequencies.

⁵ Δk was calculated in Ref. 2.

⁶K. Huang, Proc. Roy. Soc. (London) **A208**, 308 (1951).

⁷H. Poulet, Ann. Phys. (Paris) **10**, 908 (1955).

⁸D. A. Kleinman, Phys. Rev. **126**, 1977 (1962).

⁹R. Loudon, Advan. Phys. **13**, 423 (1964); **14**, 621(E) (1965), has discussed the symmetry properties of d_E and d_Q . In the present experiment, some of the crystal symmetry requirements were confirmed with IR and visible polarizers.

¹⁰For a thorough discussion of the computation of the intensity of Raman scattering by LO and TO phonons, see Ref. 9, Sec. 2.4.

¹¹Another possible solution is $C = +0.09 \pm 0.01$. This solution was discarded because it produces a functional form for the nonlinear susceptibility which is in complete disagreement with both the spontaneous forward Raman scattering intensity spectrum and with the intensities in the present experiment.

¹²R. C. Miller, Appl. Phys. Letters **5**, 17 (1964).

DECAY MODES OF O¹⁶ GIANT RESONANCE STATES*

R. O. Owens[†] and J. E. E. Baglin

Electron Accelerator Laboratory, Yale University, New Haven, Connecticut

(Received 21 November 1966)

A Ge(Li) detector has been used to observe de-excitation γ rays from O¹⁵ and N¹⁵ following the photodisintegration of O¹⁶ at giant resonance energies. Significant branching to the $(\frac{1}{2}^+, \frac{5}{2}^+)$ states near 5 MeV implies a departure from a single-particle, single-hole $E1$ absorption process.

The single-particle, single-hole model of the giant dipole resonance of O¹⁶ predicts the nature of the final residual states available in O¹⁵ and N¹⁵ following a (γ, n) or (γ, p) event. The dominant $E1$ excitations in O¹⁶ involve the promotion of a single nucleon from the $1p_{3/2}$ or $1p_{1/2}$ state to an excited $2s$ or $1d$ state. Thus, in the absence of residual interactions which could recouple the excited nucleon to the core, the final state must have a pure $(1p_{3/2})^{-1}$ or $(1p_{1/2})^{-1}$ hole configuration. The distribution of strength of such hole states has been experimentally studied and it has been established¹ that over 90% of their strength is to be found in the $\frac{1}{2}^-$ ground states and the $\frac{3}{2}^-$ states at 6.33 MeV (N¹⁵) and 6.16 MeV (O¹⁵).

If other, more complex, configurations than these are present in the giant resonance states, it becomes possible to populate with significant strength other residual states, of which the positive-parity $(\frac{1}{2}^+, \frac{5}{2}^+)$ states near 5 MeV are the lowest. Observation of branching to the positive-parity states would therefore indicate the need to consider at least two-particle, two-hole excitations or multipoles other than $E1$

in the theoretical study of the O¹⁶ giant resonance.

A direct way to study the decay branching is to observe the γ -ray spectrum produced by de-excitation of residual states of N¹⁵ and O¹⁵. In present work, a 6-cc Ge(Li) gamma detector was used to carry out a survey of the cross sections for the (γ, n_3) , the (γ, p_3) , and the $[(\gamma, n_{1,2}) + (\gamma, p_{1,2})]$ processes at excitation energies in the giant resonance region. A hardened thin-target bremsstrahlung beam from the Yale Electron Linac irradiated a water target, and the detector was located at 135° to the beam. The incident x-ray flux was monitored with an NBS type-P2 ionization chamber. Electronic pile-up of unwanted low-energy pulses during the beam burst was largely eliminated by filtering low-energy γ rays and electrons from the beam incident on the detector and by using relatively fast linear electronics.

A typical spectrum is shown in Fig. 1. It displays the 30-keV resolution which applied during the presently reported work (although better resolution is currently in use for further work). The spectrum contains double-escape